Interaction and Multiscale Mechanics, *Vol. 6, No. 2 (2013) 211-235*
DOI: http://dx.doi.org/10.12989/imm.2013.6.2.211

Incompressible smoothed particle hydrodynamics modeling of thermal convection

Burniadi Moballa, Ming-Jyh Chern* and Ernest Odhiambo

Department of Mechanical Engineering, National Taiwan University of Science and technology
43 Sec. 4 Keelung Road, Taipei 10607, Taiwan

(Received March 12, 2013, Revised March 28, 2013, Accepted May 7, 2013)

Abstract. An incompressible smoothed particle hydrodynamics (ISPH) method based on the incremental pressure projection method is developed in this study. The Rayleigh-Bénard convection in a square enclosure is used as a validation case and the results obtained by the proposed ISPH model are compared to the benchmark solutions. The comparison shows that the established ISPH method has a good performance in terms of accuracy. Subsequently, the proposed ISPH method is employed to simulate natural convection from a heated cylinder in a square enclosure. It shows that the predictions obtained by the ISPH method are in good agreements with the results obtained by previous studies using alternative numerical methods. A rotating and heated cylinder is also considered to study the effect of the rotation on the heat transfer process in the enclosure space. The numerical results show that for a square enclosure at , the addition of kinetic energy in the form of rotation does not enhance the heat transfer process. The method is also applied to simulate forced convection from a circular cylinder in an unbounded uniform flow. In terms of results, it turns out that the proposed ISPH model is capable to simulate heat transfer problems with the complex and moving boundaries.

Keywords: incompressible smoothed particle hydrodynamics (ISPH); incremental pressure projection; meshfree; natural convection; mixed convection

1. Introduction

During the course of more than 35 years, since its inception by Gingold and Monaghan (1977) and, independently, by Lucy (1977), Smoothed Particle Hydrodynamics (SPH) method has ventured many fields of application beyond the original intention in astrophysics. Recent review articles by Liu and Liu (2010), Monaghan (2012) reported the diverse applications of the SPH method and showed the capability of the method to handle complex physical problems. In the field of heat transfer, many works have been carried out to apply SPH to heat conduction problems pioneered by the work of Cleary and Monaghan (1999). However, only a few attempts have been made to apply SPH to convection problems despite the importance of the phenomena.

The first application of SPH method to convection problem dates back to Kum *et al.* (1995) who studied the Rayleigh-Bénard convection problem using a fully compressible fluid model. Applying Monaghan’s (1992) kernel function, periodic condition for lateral boundaries, and the

*Corresponding author, Professor, E-mail: mjchern@mail.ntust.edu.tw

http://www.techno-press.org/?journal=imm&subpage=7 ISSN: 1976-0426 (Print), 2092-6200 (Online)

ideal gas equation of state, they were able to predict the critical Rayleigh number close to the value reported by Chandrasekhar (1961) for an infinitely long fluid layer. They stated that the deviation can be attributed to the different models employed in both studies where Chandrasekhar (1961) used Boussinesq approximation.

Another effort to apply the SPH method to natural convection problems was done by Cleary (1998) who used a weakly compressible SPH model. He implemented Boussinesq approximation by simply replacing the body force term in the momentum equation. For the differentially heated cavity problem, he showed that the average Nusselt number predicted by the SPH method and Fastflo finite element solver were in good agreement at low and moderate Rayleigh numbers. However, discrepancies existed in results at high Rayleigh numbers from both methods. Cleary (1998) also studied Rayleigh-Bénard convection in an infinitely long fluid layer where he also used periodic boundary conditions for the lateral boundaries. However, he predicted the critical Rayleigh number which was higher than previous works.

Szewc *et al.* (2011) proposed a non-Boussinesq model which was also based on the weakly compressible SPH method and applied the method to the differentially heated cavity problem. In the Boussinesq regime, they showed that the velocity profile at the midplane and the local Nusselt number profile at the cold surface were in good agreement with the reference data. However, the average values of Nusselt number predicted by the SPH method for all Rayleigh numbers simulated were underestimated by 4% on average in comparison with results from previous works. However, the SPH model developed by Szewc *et al.* (2011) treated differently the density variation caused by heat transfer and continuity equation. In the conventional weakly compressible SPH, density is allowed to change following the continuity equation and then used to calculate pressure by the equation of state. In contrast, their model used the volume of particle obtained from the SPH summation equation, instead of the density, to calculate pressure. In their model, density was only a function of temperature and only appeared in the momentum conservation and thermal diffusion equation.

The Lagrangian and meshfree nature of SPH has become the key advantages when dealing with problems which may involve complex geometry, large deformation, moving discontinuity, or material interface. In some applications, those flow phenomena are coupled with heat transfer like the non-isothermal sloshing problem found in the fuel tank of a space shuttle or liquid metal flow in casting. SPH offers an easy way to discretize a continuum, whether it is a fluid or solid, using particles. This feature also makes it a suitable candidate to solve complex solid-fluid interaction problem coupled with heat transfer from fluid to solid found in turbomachine.

In the present work, an incompressible SPH method based on the incremental pressure projection is developed. We applied the method to simulate natural, forced, and mixed convection cases. Boussinesq approximation is adopted when simulating the natural and mixed convection cases. We chose two-dimensional Rayleigh-Bénard convection in a square enclosure with isothermal horizontal boundaries and adiabatic lateral boundaries as the validation case. The method was also employed to simulate natural convection from an isothermal horizontal circular cylinder in a square enclosure. Situations where the cylinder is rotating were also simulated to study the effect of the forced rotation on the heat transfer process. For the forced convection case, we studied the uniform flow past a hot isothermal circular cylinder at $Re = 40$.

2. Mathematical formulae and numerical model

2.1 Governing equations

The three convection problems, natural, mixed, and forced convections, considered in the present work have different forms of governing equations. For the natural and mixed convections, as the result of adopting Boussinesq approximation, the body force term is present, although the non-dimensional groups are different, while there is no body force term for the forced convection. Moreover, there are different forms of non-dimensional Boussinesq equations according to velocity scales employed in the non-dimensionalization process. Therefore, it is convenient to write the governing equations in non-dimensional forms as

$$\nabla \cdot \mathbf{u} = 0 \tag{1}$$

$$\frac{D\mathbf{u}}{Dt} = -\nabla p + C_1 \nabla^2 \mathbf{u} + C_2 \theta \tag{2}$$

$$\frac{D\theta}{Dt} = C_3 \nabla^2 \theta \tag{3}$$

where C_1, C_2, and C_3 are coefficients which represent non-dimensional groups that emerge as a result of the non-dimensionalization process.

For the natural convection case, Gray and Giorgini (1976) discussed the choice of the velocity scale and suggested the use of the velocity scale, $U = \sqrt{g\beta\left(T_H - T_C\right)L}$. Using the velocity scale, we can define non-dimensional variables listed in Table 1. The resulting formulae for C_1, C_2, and C_3 can be seen in Table 2.

For the mixed convection case, $U = \omega r$ is used as the characteristic velocity. Adopting same definitions of non-dimensional variables as in Table 1, the formulae for the coefficients can be derived using the same process as in the natural convection case. The results are also listed in Table 2.

For the forced convection case, the free stream velocity is adopted as the characteristic velocity. Because there is no body force, the coefficient C_2 is equal to zero. Hence, the Navier-Stokes and the thermal diffusion equations are uncoupled. The other two coefficients, C_1 and C_3, are defined as shown in Table 2.

Table 1 Formulae for the coefficients in the non-dimensional governing equations

Coefficient	Natural convection	Mixed convection	Forced convection
Coefficient of viscous term	$C_1 = \sqrt{\frac{Pr}{Ra}}$	$C_1 = \frac{1.0}{Re}$	$C_1 = \frac{1.0}{Re}$
Coefficient of body force term	$C_2 = 1.0$	$C_2 = \frac{Ra}{PrRe^2}$	0.0
Coefficient of temperature Laplacian	$C_3 = \frac{1.0}{\sqrt{PrRa}}$	$C_3 = \frac{1.0}{RePr}$	$C_3 = \frac{1.0}{RePr}$

Table 2 Comparison of average Nusselt numbers at the bottom boundary of the Rayleigh-Bénard convection in a square enclosure

Rayleigh number	Ouertatani *et al.* (2008)	Present study
10^4	2.158	2.159
10^5	3.910	3.888
10^6	6.309	6.317

Throughout this study, we use SPH gradient and divergence operators denoted, respectively, as

$$\langle \nabla \phi \rangle_i = \sum_j \frac{m_j}{\rho_j} \left(\phi_j - \phi_i \right) \nabla W_{ij} \tag{4}$$

and

$$\langle \nabla \cdot \mathbf{v} \rangle_i = \sum_j \frac{m_j}{\rho_j} \left(\mathbf{v}_j - \mathbf{v}_i \right) \cdot \nabla W_{ij} \tag{5}$$

where ϕ_i and $\mathbf{v}_i$ denotes scalar and vector variables of *i*th particle.

When the above operators are used in conjunction with the kernel gradient correction proposed by Bonet and Lok (1999), their accuracies are significantly improved. This issue has been studied in detail by Oger *et al*. (2007). Although it appears that they flout the coherence principle and infringe on the reciprocity principle, above operators give better performance compared to the symmetric operators. In the context of incompressible SPH, Xu *et al.* (2009) has successfully applied above operators to simulations of Taylor-Green vortices.

The corrected kernel gradient, $\tilde{\nabla} W_{ij}$, is given by

$$\tilde{\nabla} W_{ij} = \mathbf{L}_i \nabla W_{ij} \tag{6}$$

where $\mathbf{L}_i$ is the kernel gradient correction. Following Bonet and Lok (1999), the formula for $\mathbf{L}_i$ is denoted as

$$\mathbf{L}_i = \mathbf{M}_i^{-1} \tag{7}$$

where

$$\mathbf{M}_i = \sum_j \frac{m_j}{\rho_j} \nabla W_{ij} \otimes (\mathbf{x}_i - \mathbf{x}_j) \tag{8}$$

The Laplacian operator applied in this work is similar to the one suggested by Brookshaw (1985). Morris *et al.* (1997) successfully applied this form of Laplacian to viscous flow simulations. Similar formulation is also used by Cummins and Rudman (1999) and Xu *et al.* (2009) to formulate the discrete pressure Poisson equation of incompressible SPH method. The Laplacian operator formulae for a scalar variable, ϕ, and a vector variable, v, of the *i*th particle are denoted, respectively, as

$$\left\langle \nabla^2 \phi \right\rangle_i = \sum_j \frac{m_j}{\rho_j} \left(\frac{2.0 \mathbf{x}_{ij} \cdot \nabla_i W\left(\mathbf{x}_i - \mathbf{x}_j\right)}{\left|\mathbf{x}_{ij}\right|^2} \right) \left(\phi_i - \phi_j\right) \tag{9}$$

and

$$\left\langle \nabla^2 \mathbf{v} \right\rangle_i = \sum_j \frac{m_j}{\rho_j} \left(\frac{2.0 \mathbf{x}_{ij} \cdot \nabla_i W\left(\mathbf{x}_i - \mathbf{x}_j\right)}{\left|\mathbf{x}_{ij}\right|^2} \right) \left(\mathbf{v}_i - \mathbf{v}_j\right) \tag{10}$$

Applying the suitable operator, we can obtain the SPH discretized momentum equation and the thermal diffusion equation denoted, respectively, as

$$\begin{aligned} \frac{D\mathbf{u}_i}{Dt} = &-\sum_j \frac{m_j}{\rho_j} \left(p_j - p_i\right) \nabla_i W\left(\mathbf{x}_i - \mathbf{x}_j\right) + \\ &C_1 \sum_j \frac{m_j}{\rho_j} \left(\frac{2.0 \mathbf{x}_{ij} \cdot \nabla_i W\left(\mathbf{x}_i - \mathbf{x}_j\right)}{\left|\mathbf{x}_{ij}\right|^2} \right) \left(\mathbf{u}_i - \mathbf{u}_j\right) + C_2 \theta_i \mathbf{j} \end{aligned} \tag{11}$$

and

$$\frac{D\theta_i}{Dt} = C_3 \sum_j \frac{m_j}{\rho_j} \left(\frac{2.0 \mathbf{x}_{ij} \cdot \nabla_i W\left(\mathbf{x}_i - \mathbf{x}_j\right)}{\left|\mathbf{x}_{ij}\right|^2} \right) \left(\theta_i - \theta_j\right) \tag{12}$$

2.2 Kernel function

The choice of kernel function is of paramount importance in SPH since the stability of SPH strongly depends upon the second derivative of the kernel. A detailed description on the method of constructing kernel function can be found in the monograph by Liu and Liu (2003). In this study, we apply the quintic spline kernel function identical to the one adopted by Morris *et al.* (1997). The formula of the quintic spline is denoted as

$$f(s) = \begin{cases} (3-s)^5 - 6(2-s)^5 + 15(1-s)^5, & 0 \le s < 1; \\ (3-s)^5 - 6(2-s)^5, & 1 \le s < 2; \\ (3-s)^5, & 2 \le s < 3; \\ 0, & s \ge 3; \end{cases} \tag{13}$$

and the normalized kernel function in two dimensions is denoted as

$$W = \frac{7}{478 \pi h^2} f \tag{14}$$

Sigalotti *et al.* (2003) compared the performance of the quintic spline kernel and the cubic spline kernel for the case of plane Poiseuille flow where the effect of the viscous term is significant and found that quintic spline kernel gave better results.

2.3 Boundary treatment

SPH has an isotropic stencil that becomes truncated near a wall. A truncated kernel will cause an incorrect gradient evaluation for a near-wall particle and could drive a particle to penetrate the wall. A technique using edge and dummy particles identical to the one used by Lee *et al.* (2008) is employed in this study. A layer of particles is placed exactly at the boundary. These particles, the so-called edge particles, follow the conservation equations, have zero velocity and do not move. Each edge particle corresponds to a number of dummy particles placed in line beyond it so that the wall thickness is about equal to the support length. This setting is used to maintain the uniformity of particle distribution. Dummy particles do not follow the conservation equations. Values of field variables of dummy particles are determined according to the relevant boundary condition at the wall.

In order to enforce the non-slip boundary condition, dummy particles are assigned the same velocity value as the corresponding edge particles. Homogenous Neumann boundary condition on pressure can be enforced by assigning to dummy particles the same pressure value as the corresponding edge particle, while letting the pressure of edge particles to evolve following the governing equations.

An adiabatic boundary condition is implemented by assigning to dummy particles the same temperature value as the corresponding edge particle. Meanwhile, the temperature of the corresponding edge particle is evolved following the governing equations. This method will give a zero temperature gradient across the boundary. An isothermal boundary can be implemented by keeping temperatures of edge particles constant while temperatures of the corresponding dummy particles are extrapolated using a first order Taylor expansion based on the temperature gradient of the edge particle.

For an external flow problem, like the flow past a circular cylinder, the domain basically extends to infinity. However, in order to be feasible, the domain used in the simulation must be finite. Therefore it is necessary to truncate the domain and to define boundaries and boundary conditions that would take into account the effects of the finite domain to the solution. In grid based methods, it is a common practice to use rectangular domain when simulating external flow. One boundary, usually the left vertical boundary, is defined as the inlet with Dirichlet boundary condition on velocity. The opposite boundary is defined as the outlet with Dirichlet boundary condition on pressure. The Neumann boundary conditions on pressure and velocity are usually prescribed at the lateral boundaries.

In the present work, we only defined boundary conditions for inlet and outlet boundaries and left the lateral boundaries without any prescribed condition. We believe that the SPH method can handle the domain truncation well without any need for prescribing the boundary condition that will take into account the effect of the finite domain. The inlet and outlet boundaries are implemented by defining the inlet and outlet regions beyond the domain boundaries whose widths are equal to support length. This method is similar to the one proposed by Lastiwka *et al.* (2009). However, instead of introducing particles at the inlet and destroying them at the outlet, as proposed by Lastiwka *et al.* (2009), we simply drag back the particles that have moved beyond the outlet region into the inlet region. We believe that mass conservation is better treated this way. Moreover, this method is easier to implement compared to the former.

2.4 Incremental pressure projection

Using the first order backward difference in time, we can write the discretized momentum conservation equation in the following form

$$\frac{\mathbf{u}^{n+1}-\mathbf{u}^{n}}{\Delta t}=-\nabla p^{n+1}+C_1\nabla^2\mathbf{u}^n+C_2\theta\mathbf{j} \tag{15}$$

Defining the auxiliary velocity field, u^*, and writing the pressure at the next time step, p^{n+1}, as

$$p^{n+1}=p^n+\delta p \tag{16}$$

the momentum conservation equation can be split into

$$\frac{\mathbf{u}^{*}-\mathbf{u}^{n}}{\Delta t}=-\nabla p^{n}+C_1\nabla^2\mathbf{u}^n+C_2\theta\mathbf{j} \tag{17}$$

$$\frac{\mathbf{u}^{n+1}-\mathbf{u}^{*}}{\Delta t}=-\nabla\delta p \tag{18}$$

Taking divergence on both sides of Eq. (18), the pressure Poisson equation in the following form is obtained

$$\nabla^2\delta p=\frac{\nabla\cdot\mathbf{u}}{\Delta t} \tag{19}$$

It was Chorin (1968), Temam (1968) that originally suggested the projection method to solve the Navier-Stokes equation. The idea of incorporating pressure gradient from the previous time step to increase the stability was first put forth by Goda (1979) leading to above decomposition.
Applying SPH operators defined above, we obtain the SPH pressure Poisson equation denoted as

$$\sum_j\frac{m_j}{\rho_j}\left(\frac{2.0\mathbf{x}_{ij}\cdot\nabla_iW\left(\mathbf{x}_i-\mathbf{x}_j\right)}{\left|\mathbf{x}_{ij}\right|^2}\right)\left(\delta p_i-\delta p_j\right)=\frac{1}{\Delta t}\sum_j\frac{m_j}{\rho_j}\left(\mathbf{u}_j-\mathbf{u}_i\right)\cdot\nabla_iW\left(\mathbf{x}_i-\mathbf{x}_j\right) \tag{20}$$

Assembling SPH pressure Poisson equations for all fluid and edge particles, a system of linear equation in the form of

$$\mathbf{Ax}=\mathbf{B} \tag{21}$$

where

$$A(i,j)=-\frac{m_j}{\rho_j}\left(\frac{2.0\mathbf{x}_{ij}\cdot\nabla_iW\left(\mathbf{x}_i-\mathbf{x}_j\right)}{\left|\mathbf{x}_{ij}\right|^2}\right) \tag{22}$$

$$A(i,i)=\sum_j \frac{m_j}{\rho_j}\left(\frac{2.0\mathbf{x}_{ij}\cdot\nabla_i W\left(\mathbf{x}_i-\mathbf{x}_j\right)}{\left|\mathbf{x}_{ij}\right|^2}\right) \tag{23}$$

and

$$B\left(i\right)=\frac{1}{\Delta t}\sum_j \frac{m_j}{\rho_j}\left(\mathbf{u}_j-\mathbf{u}_i\right)\cdot\nabla_i W\left(\mathbf{x}_i-\mathbf{x}_j\right) \tag{24}$$

is generated.

For cases where wall boundaries are presented, a homogenous Neumann boundary condition on pressure denoted as

$$\mathbf{n}\cdot\nabla\delta p=0\big|_\Gamma \tag{25}$$

must be imposed when solving the pressure Poisson equation. Under the method of edge and dummy particles, this condition implies that the pressures of dummy particles must have the same value as the corresponding edge particles. This condition can be easily incorporated by modifying the coefficient matrix of the corresponding edge particles. Using this method, the homogenous Neumann boundary condition will be automatically satisfied when the system of linear equation is solved. In this study, general minimal residual (GMRES) method is used to solve the system of linear equation for all simulated cases.

The pressure field obtained using this method could suffer from the so-called spurious pressure mode. Monaghan (1989) has derived a formula to smooth out the velocity field so that the particle moves with a velocity that is close to the average velocity in its neighbourhood. In the present work, a similar formula is applied to smooth out the pressure field and remove the spurious pressure mode. When it is applied to the pressure, the formula is denoted as

$$\overline{p}_i=p_i+\sum_j \frac{m_j}{\rho_j}\left(p_j-p_i\right)W\left(\mathbf{x}_i-\mathbf{x}_j\right) \tag{26}$$

where $\overline{p}_i$ is the smoothed pressure.

2.5 Tensile instability

Incompressibility condition requires that a particle has a constant volume. In a Lagrangian method such as SPH, it means that the particle distribution should be uniform. If particles are closely clustered in a region of the flow domain and leaving other region void of particle, we can no longer hold that the volumes of those closely clustered particles are constant. It is noted by Hu and Adams (2007), only if a discrete velocity-divergence-free condition is enforced, particle clustering may occur due to the spatial truncation error of the discretization scheme.

In this work, we employ the particle shifting strategy proposed by Xu *et al*. (2009) to prevent particle clustering. The idea of this method consists in shifting the fluid particles a little bit away from their streamlines and corrects the field variables according to the first order Taylor expansion.

The direction and amount of the shift is determined by the local arrangement of neighbouring particles under the support region. We also adopt the formula in Xu *et al*. (2009) to determine the shifting vector and position shift.

2.6 Time step criteria

There are two widely used time step criteria in the context of incompressible SPH that limit the choice of time step size. Cummins and Rudman (1999) proposed a CFL stability constraint expressed by

$$\Delta t \le \frac{0.25h}{U} \tag{27}$$

for resolutions less than 50 × 50 and a viscous diffusion condition-based constraint denoted as

$$\Delta t \le 0.125 Re h^2 \tag{28}$$

for higher resolutions. On the other hand, Shao and Lo (2003) used initial particle spacing instead of smoothing length, h, in the CFL condition and proposed a smaller constant of 0.1 leading to a stringent requirement.

2.7 Solution algorithm

The solution algorithm based on the above numerical schemes is described in the following steps

1. Calculate auxiliary velocities using the momentum equation including the pressure gradient from previous time step and the body force term

$$\mathbf{u}_i^* = \mathbf{u}_i^n + \Delta t\left[-\nabla p_i^{\,n} + C_1\left(1.5\nabla^2\mathbf{u}_i^{\,n} - 0.5\nabla^2\mathbf{u}_i^{\,n-1}\right) + C_2\left(1.5\theta_i^n - 0.5\theta_i^{n-1}\right)\mathbf{j}\right] \tag{29}$$

The second order Adam-Bashforth scheme is applied to the viscous and body force terms to increase the accuracy.

2. Calculate the mass residual

$$D_i = \nabla \cdot \mathbf{u}_i^* \tag{30}$$

3. Assemble the SPH pressure Poisson equation (Eq. (19)) and solve for δp.
4. Calculate pressure at the next time step

$$p^{n+1} = p^n + \omega\delta p \tag{31}$$

5. Calculate the gradient of $\delta p$and use it to calculate the velocity at the next time step

$$\mathbf{u}_i^{n+1} = \mathbf{u}_i^* - \Delta t\nabla\delta p \tag{32}$$

6. Calculate the Laplacian of temperature and use it to update the temperature at the next time step

$$\theta_i^{n+1} = \theta_i^n + C_3\left(1.5\nabla^2\theta_i^n - 0.5\nabla^2\theta_i^{n-1}\right) \tag{33}$$

The second order Adam-Bashforth scheme is applied to the temperature Laplacian term to increase the accuracy.

7. Update the position of the particle

$$\mathbf{x}_i^{n+1} = \mathbf{x}_i^n + \Delta t\left(1.5\mathbf{u}_i^{n+1} - 0.5\mathbf{u}_i^n\right) \tag{34}$$

8. Apply particle shifting strategy to prevent tensile instability and correct field variables using Taylor expansion.

3. Results and discussion

3.1 Validation of the numerical scheme

The Rayleigh-Bénard convection in a square enclosure was simulated in this study for validation purposes. The horizontal walls were in isothermal conditions. The presence of adiabatic lateral walls serves as a test bed for the implementation of the SPH boundary condition. Recently, benchmark solutions for this case at various Rayleigh numbers were proposed by Ouertatani *et al.* (2008). They used a finite volume multigrid method and a fine mesh to simulate the case. Their results were used to validate the developed numerical scheme. Following Ouertatani *et al.* (2008), the reference temperature, T_{ref}, is defined as

$$T_{ref} = \frac{T_H + T_C}{2.0} \tag{35}$$

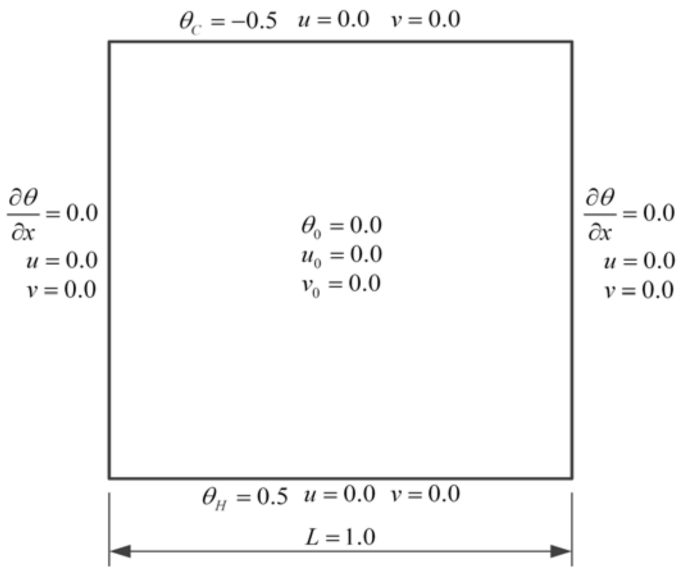

Fig. 1 Schematic of the domain and boundary conditions for the Rayleigh-Bénard convection in a square enclosure

Using the definition of reference temperature in Eq. (36), the isothermal hot and cold boundary are given by

$$\theta_H = 0.5 \quad \text{and} \quad \theta_C = -0.5$$

The schematic layout of the system is presented in Fig. 1. The Prandtl number was taken as 0.71 similar to the air property. A time step of 10^{-3} was used for all simulated Rayleigh numbers.

A particle number independence study was conducted to determine how the solution will behave with increasing number of particles and to establish the number of particles that will be used in the validation study. A Rayleigh number of 10^5 was chosen for the study. The results of the particle number independence study are presented in Fig. 2 in terms of the local Nusselt number profile at the bottom wall. It is interesting to note that in this case the solution obtained using a smaller number of particles does not show a significant difference compared to the one obtained using a larger number of particles except at corners of the domain.

Simulations were carried out at Ra = 10^4, 10^5, and 10^6. The evolution of Rayleigh-Bénard convection at Ra = 10^5 is depicted in Figs. 3(a)-(c). Streamlines and isotherms of the results are presented in Figs. 4-5, respectively. The streamlines show that the corner vortices become larger with increasing Rayleigh number. Horizontal and vertical velocity profiles at the mid plane are presented in Figs. 6-7, respectively. The velocity profiles show that results from the ISPH method are in good agreement with the benchmark solutions. Local Nusselt number profiles at the bottom boundary are presented in Fig. 8. For the local Nusselt number profiles, results predicted by the ISPH method are in good agreement with the benchmark solutions except for the slight discrepancy at higher Rayleigh number. Table 3 depicts the comparison of average Nusselt numbers at the bottom boundary due to varying Ra. The average Nusselt numbers obtained are also in good agreement with the benchmark solution.

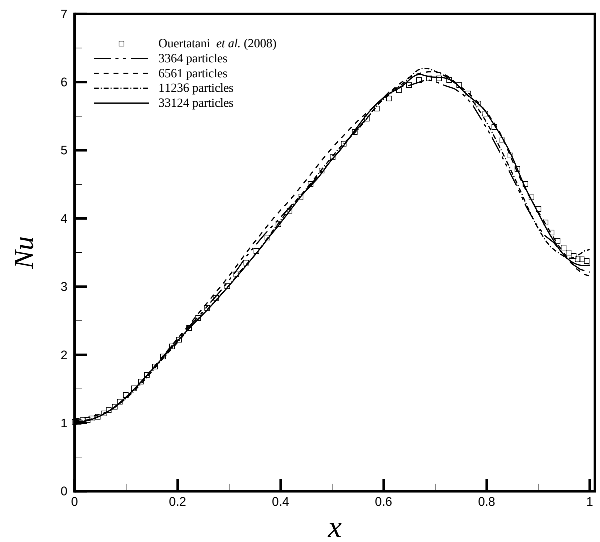

Fig. 2 Grid independence study using local Nusselt number profile at the bottom wall

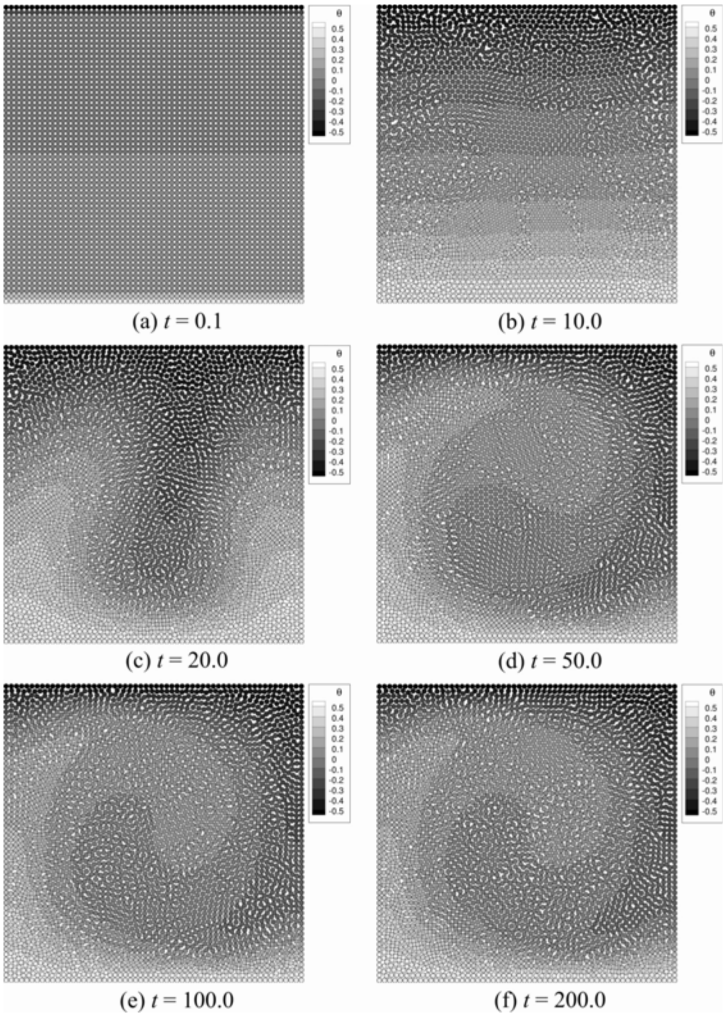

Fig. 3 The isothermal evolution of Rayleigh-Bénard convection at $Ra = 10^5$. Particles are colored by dimensionless temperature

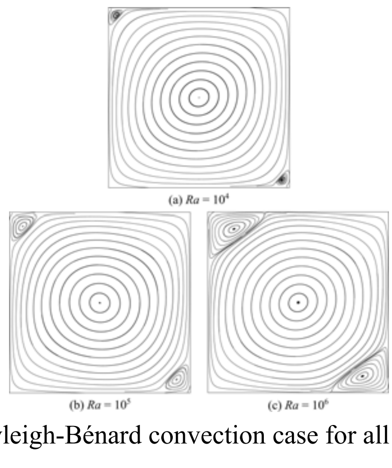

Fig.4 Streamlines of the Rayleigh-Bénard convection case for all simulated Rayleigh numbers

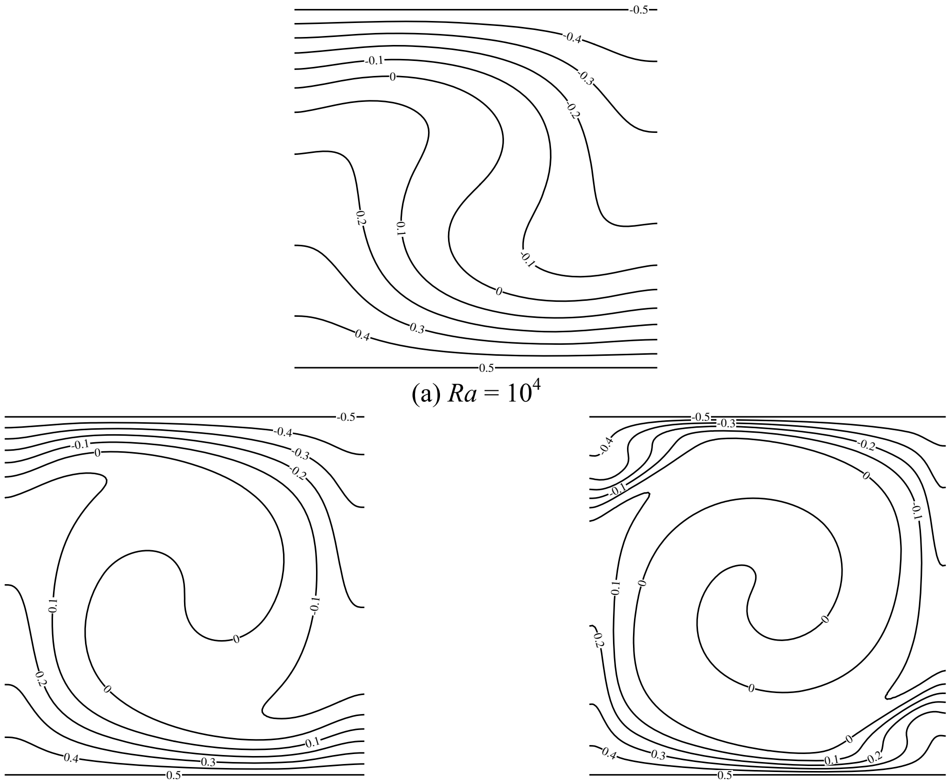

(a) $Ra = 10^4$

(b) $Ra = 10^5$

(c) $Ra = 10^6$

Fig. 5 Isotherms of the Rayleigh-Bénard convection case for all simulated Rayleigh numbers

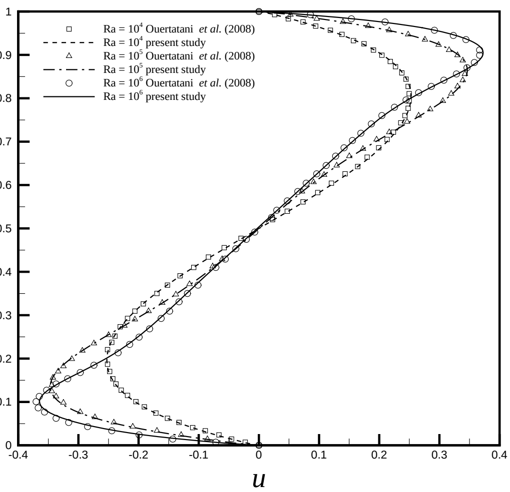

Fig. 6 Horizontal velocity profiles at the middle plane in the Rayleigh-Bénard convection case

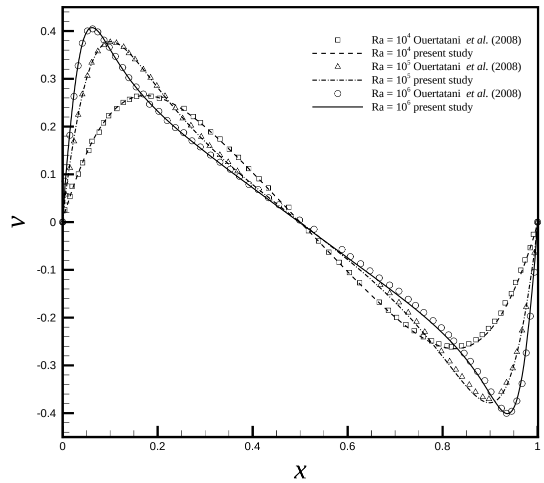

Fig. 7 Vertical velocity profiles at the middle plane in the Rayleigh-Bénard convection case

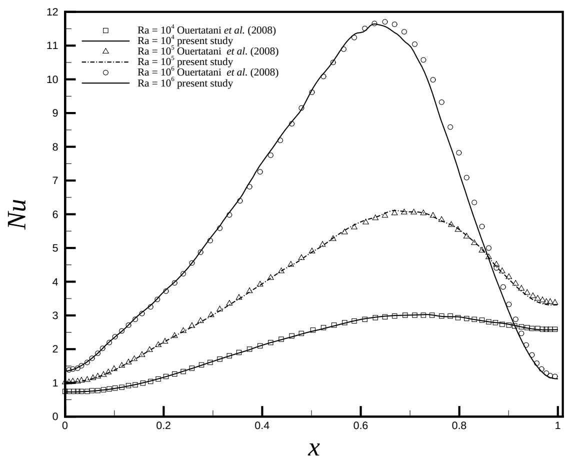

Fig. 8 Profiles of local Nusselt number along the bottom boundary in the Rayleigh-Bénard Convection case

Table 3 Average Nusselt numbers at the cylinder surface of the natural convection in a square enclosure from a heated cylinder

	$Ra = 10^4$	$Ra = 10^5$	$Ra = 10^6$
Moukalled and Acharya (1996)	2.071	3.825	6.107
Shu and Zhu (2002)	2.080	3.790	6.110
Peng *et al.* (2003)	2.080	3.790	5.960
Angeli *et al.* (2008)	2.225	3.733	6.267
Present study	2.099	3.823	6.133

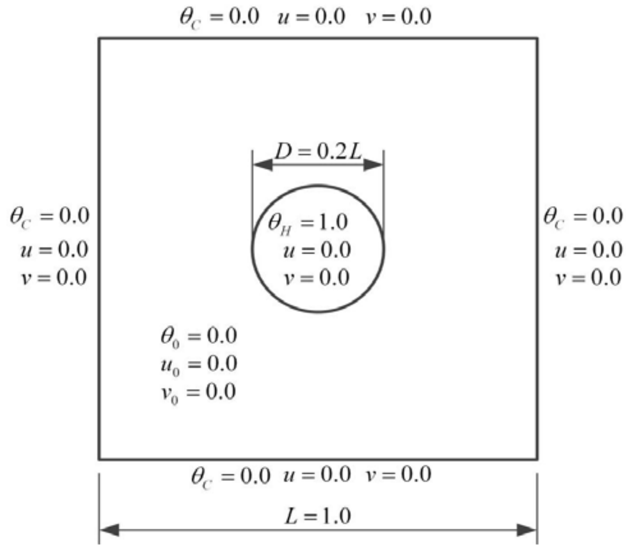

Fig. 9 Schematic of the domain and boundary conditions for the natural convection in a square enclosure from a heated cylinder

3.2 Natural convection from a heated cylinder inside a square enclosure

The phenomenon of natural convection from a heated cylinder placed at the centre of a square enclosure was simulated. The system consists of a square enclosure filled with air. Isothermal boundary conditions were given at all of the walls and a cylinder was placed at the centre of the enclosure whose surface was also in an isothermal condition but at a hotter temperature. This case was first studied numerically by Moukalled and Acharya (1996) using a finite volume method and a body fitted mesh. They used the steady state formulation of the governing equations and solved one-half of the domain arguing for the symmetric nature of the flow around the vertical axis. They performed numerical simulations for three different diameters of cylinder to enclosure width ratio and four different values of Rayleigh number ranging from 10^4 to 10^7.

Later, Shu and Zhu (2002) developed a differential quadrature method to simulate this problem. Using the differential quadrature method, they could obtain accurate solutions using relatively coarse grids. They also adopted the steady state formulation of the governing equations. The simulations were performed for Rayleigh numbers ranging from 10^4 to 10^6 and aspect ratios between 1.67 and 5.0. The results were validated against Moukalled and Acharya (1996). Another study was carried out by Peng *et al.* (2003) using the lattice Boltzmann method. The simulations were performed at the same ranges of Rayleigh numbers and aspect ratios as in Shu and Zhu (2002) and the results were also validated against Moukalled and Acharya (1996). Recently, Angeli *et al.* (2008) revisited the problem and studied not only the steady flow-field and heat transfer predictions but also the long-term behaviour of the flow regimes using the direct numerical simulation.

In the present study, the ratio of cylinder diameter to enclosure width is set as 0.2. The simulations were performed at $Ra = 10^4$, 10^5, and 10^6. The schematic of the convection problem is depicted in Fig. 9. The Prandtl number was taken equal to 0.7 in this problem. A dimensionless time step of 10^{-3} was selected for all simulations in this problem.

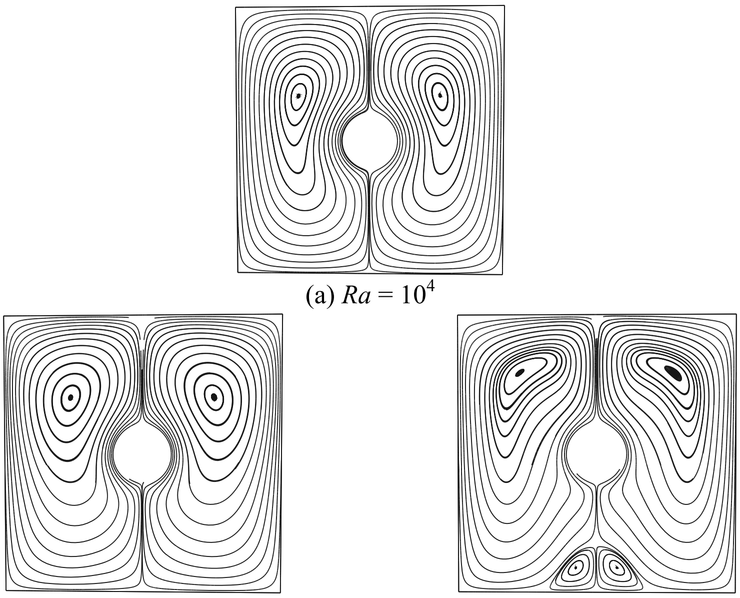

(a) $Ra = 10^4$

(b) $Ra = 10^5$ (c) $Ra = 10^6$

Fig. 10 Streamlines of the natural convection in a square enclosure from a heated cylinder for all simulated Rayleigh numbers

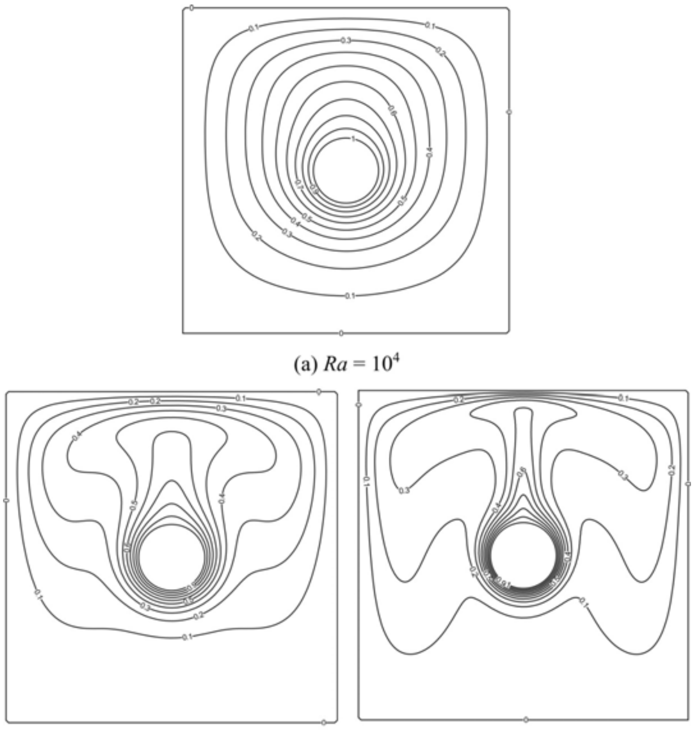

(a) $Ra = 10^4$

(b) $Ra = 10^5$ (c) $Ra = 10^6$

Fig. 11 Streamlines of the natural convection in a square enclosure from a heated cylinder for allsimulated Rayleigh numbers

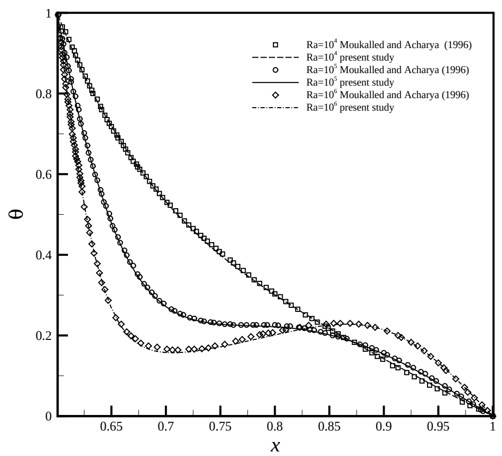

Fig. 12 Isothermal profiles at the middle plane of the natural convection in a square enclosure from a heated cylinder for all simulated Rayleigh numbers

Streamlines and isotherms of the results are presented in Figs. 10-11. The isotherms show that at low Rayleigh number, conduction dominates the heat transfer mechanism. Heat is transferred radially from the surface of the cylinder to the boundaries of the enclosure. At higher Rayleigh numbers, the density variation becomes significant, causing a substantial upward movement of the fluid, i.e. the so-called thermal plume. This upward movement is compensated by entrainments below the cylinder. Hence, convection becomes a dominant heat transfer mechanism.

Temperature profiles along the horizontal direction at the mid plane are presented in Fig. 12. At low Rayleigh number, temperature decreases monotonically with increasing distance from the cylinder surface. The phenomenon of temperature inversion emerges at higher Rayleigh numbers. At higher Rayleigh numbers, temperature drops rapidly in the vicinity of the cylinder surface and then increases slowly before it decreases again near the cold surface of the enclosure. It is like that a thermal boundary layer is formed near the wall boundaries. The figure also shows that the results from the ISPH method are in good agreement with the results from Moukalled and Acharya (1996).

Vertical velocity profiles along the horizontal direction at the middle plane are presented in Fig. 13. The profiles are steeper in the region adjacent to the cylinder surface than those in the region adjacent to the cold boundaries because the density stratification is higher in the vicinity of the cylinder than other regions in the domain. Since Moukalled and Acharya (1996) used a different velocity scale ($U = \nu/L$) in the non-dimensionalization process, the velocity from the present study must be rescaled before a comparison is made. The formula for rescaling is denoted as

$$u_2 = \sqrt{\frac{Ra}{Pr}} u_1 \tag{36}$$

where u_2 denotes the non-dimensional velocity when $U = \nu/L$ and u_1 denotes the non-dimensional velocity when $U = \sqrt{g\beta\Delta TL}$. The comparison shows that generally the results

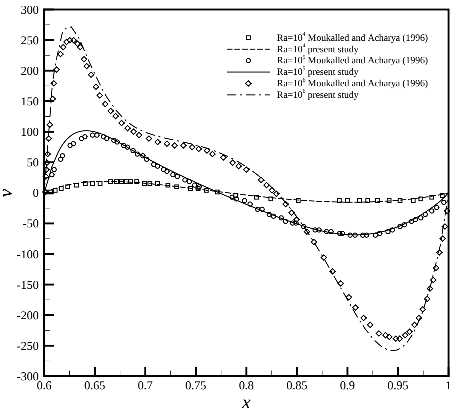

Fig. 13 Vertical velocity profiles at the middle plane of the natural convection in a square Enclosure from a heated cylinder for all simulated Rayleigh numbers

Table 4 Drag coefficient, recirculation length, and average Nusselt number at the cylinder surface for the forced convection from a circular cylinder in an unbounded uniform flow

	C_D	l_w	$\bar{N}_u$
Kim and Choi (2004)	-	-	3.23
Pan (2006)	1.51	2.18	3.23
Pacheco-Vega *et al.* (2007)	1.53	2.28	3.62
Noor *et al.* (2009)	1.51	2.26	-
Present study	1.504	2.155	3.16

from the ISPH method and the results from Moukalled and Acharya (1996) are in good agreement.

Average Nusselt numbers at the cylinder surface for all simulated Rayleigh Numbers are presented in Table 4 along with results from previous studies. On average, the relative error of the results from the present study compared to the previous studies is about 1.57%. The relative errors at low Rayleigh number (Ra = 10^4) are generally higher (2.21 % in average) compared to relative errors at higher Rayleigh Numbers.

3.3 Mixed convection in a square enclosure from a heated and rotating cylinder

A heated and rotating cylinder is also considered in this work. The rotation of the cylinder introduces forced convection to the system. While the natural convection induces symmetric flow around the cylinder, the forced flow generated by the rotation of the cylinder is unidirectional in the azimuthal direction. It is interesting to study the heat transfer phenomena under the varying ratio of buoyancy force to inertia force.

Ghaddar and Thiele (1994) studied a similar problem in a vertical rectangular enclosure using a spectral element method with a body fitted mesh. The cylinder was placed in the center of the lower half of the rectangular enclosure. The walls were in constant heat flux conditions. The ratio of the diameter of cylinder to the enclosure width was 0.2. Simulations were carried out for

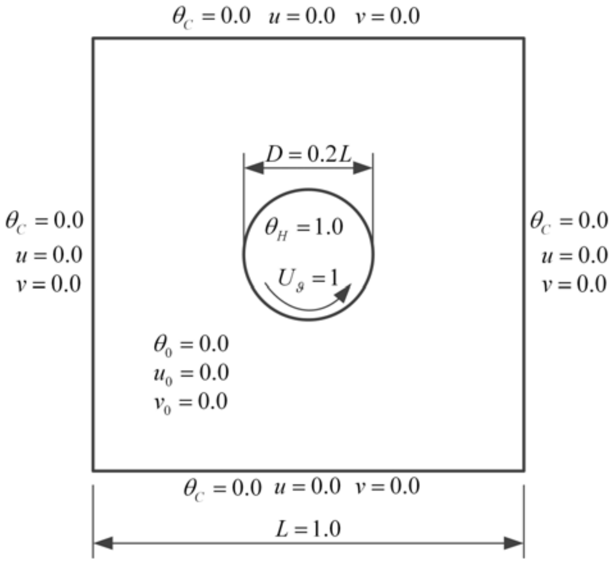

Fig. 14 Schematic of the domain and boundary conditions for the mixed convection in a squareenclosure from a heated and rotating cylinder

Ra/Re_D^2 ranging from 0.4 to 250. They concluded that the heat transfer was significantly enhanced at low Ra. They also stated that at the Reynolds number of 100.0 the flow became unsteady.

In the present study, we consider a square enclosure with the same cylinder diameter as in Ghaddar and Thiele (1994). We investigate a regime where $Ra/Re_D^2 \geq 1$. In this regime, the strength of buoyancy force is comparable to the inertia force. Simulations were carried out at Pr = 0.71 and Re_D = 100. Rayleigh number is varied from 10^4 to 10^6. The cylinder and enclosure walls are in isothermal conditions. The schematic layout of the domain and boundary conditions can be seen in Fig. 14. A dimensionless time step of 10^{-3} is chosen.

Steady streamlines and isotherms of the results at $Ra = 10^4 - 10^6$ are presented in Figs. 15-16. For $Ra = 10^4$ or $Ra/Re_D^2 = 1$, forced convection dominates the heat transfer process. The isotherms are circular and concentric similar to the case of a stationary cylinder at same Rayleigh number. The streamlines at this Rayleigh number are also circular and concentric indicating that the forced rotation dominates the flow phenomenon.

At $Ra = 5\times10^4$, the effect of buoyancy begins to emerge at the right hand side of the cylinder where the direction of the cylinder rotation is parallel to flow induced by the buoyancy force. At $Ra = 10^5$, a saddle point can be readily seen in the streamlines on the vicinity of the cylinder. In the region inside the saddle point, the forced rotation is dominant. In the region outside the saddle point, buoyancy induced flow is dominant. The saddle point moves closer to the cylinder surface with increasing Rayleigh number and the layer where the forced rotation is dominant becomes thinner. At the left hand side of the cylinder, the velocity profile reverts sharply in the radial direction. This phenomenon poses a problem of stability to the method at higher Rayleigh number. At $Ra = 10^6$, a distinct thermal plume can be seen to rise from the cylinder. The rotation convects the plume to the top left corner of the enclosure.

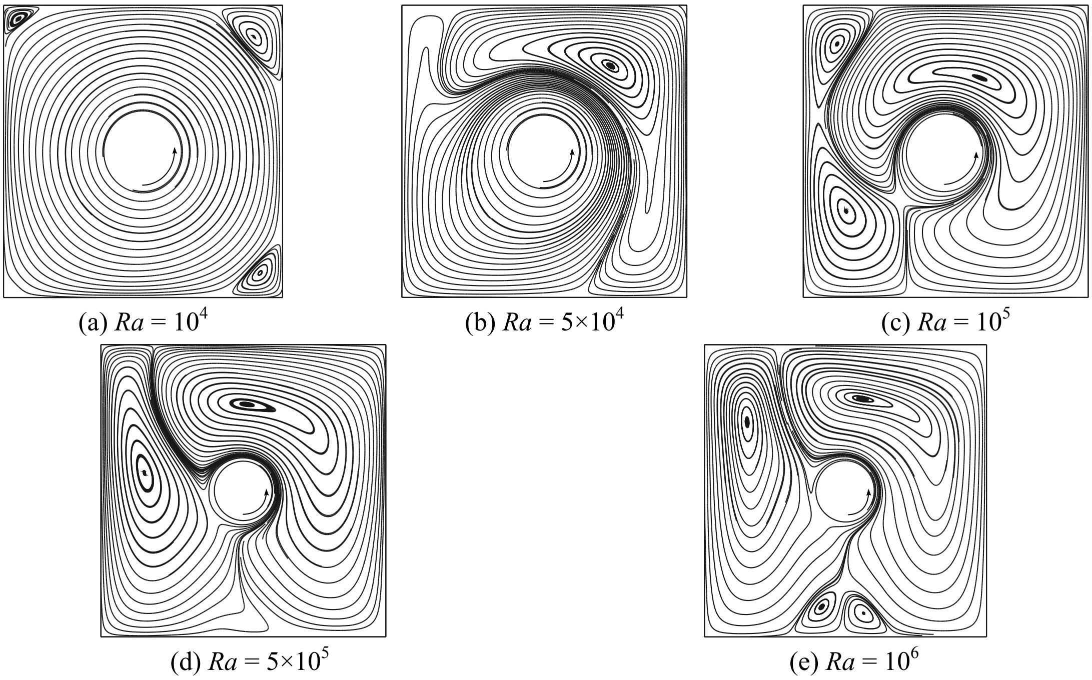

Fig. 15 Streamlines of the mixed convection in a square enclosure from a heated and rotating cylinder at ReD = 100 for all simulated Rayleigh numbers

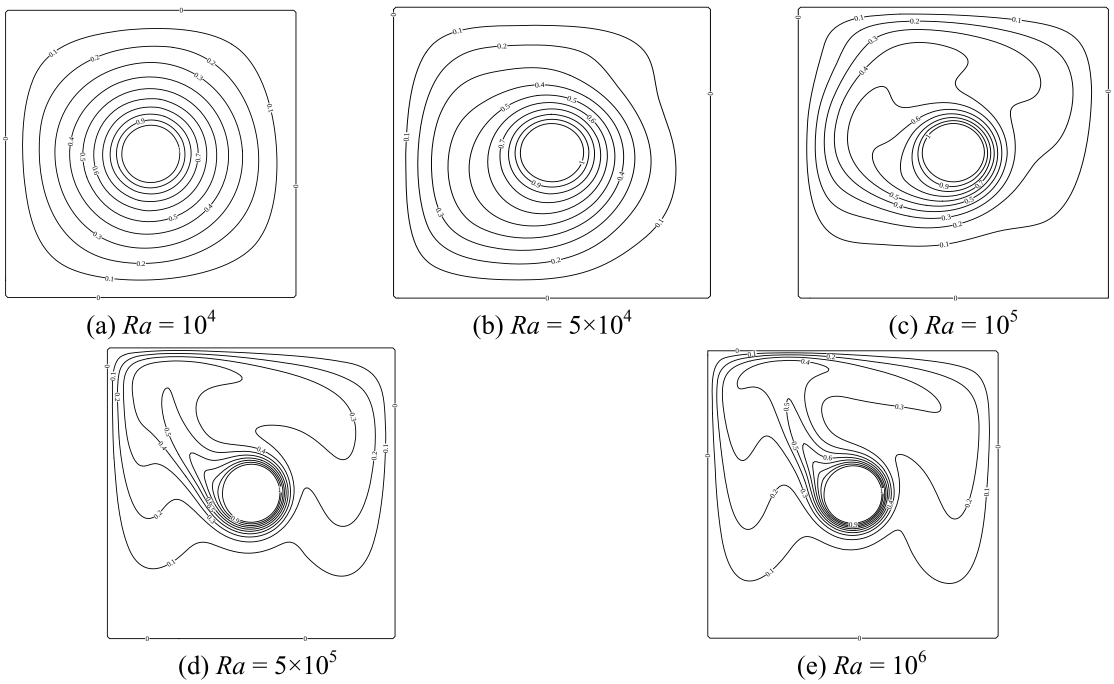

Fig. 16 Isotherms of the mixed convection in a square enclosure from a heated and rotating cylinderat ReD = 100 for all simulated Rayleigh numbers

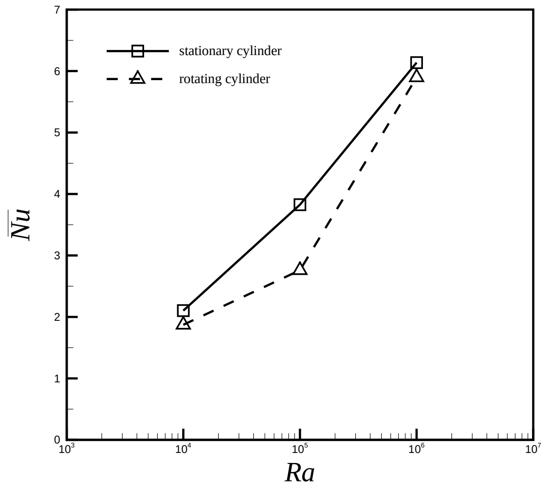

Fig. 17 The comparison of average Nusselt numbers at the cylinder surface between stationary and rotating cylinder cases at ReD = 100

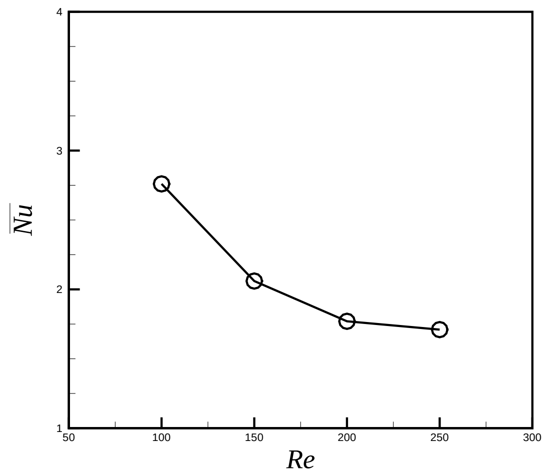

Fig. 18 The variation of average Nusselt number at the cylinder surface with increasing Reynolds number at $Re = 10^5$

Fig. 17 depicts a comparison of average Nusselt number at the cylinder surface between the stationary and rotating cylinders. The figure shows that, for a square enclosure, the average Nusselt numbers of the rotating cylinder are lower than the stationary cylinder. The variation of average Nusselt number at the cylinder surface with respect to constant Rayleigh number at $Ra = 10^5$ is presented in Fig. 18. It is shown in the figure that the average Nusselt number drops when the Reynolds number increases. All of the results presented above indicate that at $Ra/Re_D^2 \geq 1$, the forced rotation does not enhance the heat transfer process.

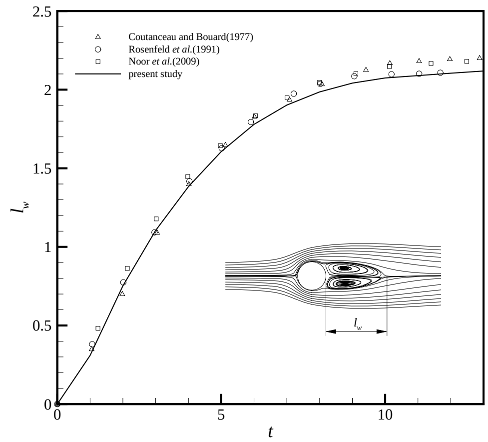

Fig. 19 The time history of recirculation length at *Re* = 40 compared to previous works by Coutanceau and Bouard (1977), Rosenfeld *et al.* (1991), Chern *et al.* (2006), Noor *et al.* (2009)

Table 5 Drag coefficient, recirculation length, and average Nusselt number at the cylinder surface for the forced convection from a circular cylinder in an unbounded uniform flow

	C_D	l_w	$\overline{N}_u$
Kim and Choi (2004)	-	-	3.23
Pan (2006)	1.51	2.18	3.23
Pacheco-Vega *et al.* (2007)	1.53	2.28	3.62
Noor *et al.* (2009)	1.51	2.26	-
Present study	1.504	2.155	3.16

3.4 Forced convection from a cylinder in a uniform flow

We simulate the forced convection from a hot isothermal circular cylinder in an unbounded uniform flow at *Re* = 40. At *Re* = 40, the flow is laminar with steady separation. A pair of steady counter rotating vortices is formed in the near wake. The time history of the recirculation length obtained in the present work compared to previous works is depicted in Fig. 19. The comparison of drag coefficient, recirculation length and average Nusselt number at the cylinder surface in the steady state with previous works is listed in Table 5. We can see from those comparisons that the results obtained by current ISPH method are in good agreement with previous results.

4. Conclusions

In the present study, an incompressible SPH method based on incremental pressure correction has been developed. The pressure Poisson equation resulting from the decomposition process is solved with a homogenous Neumann boundary condition. Rayleigh-Bénard convection in a square enclosure is simulated to validate the proposed method. The comparison of the results with the benchmark solution obtained by the finite volume multigrid method shows that the present ISPH method is able to achieve a comparable accuracy with a well-established numerical model. In this case, the SPH method is also able to reveals the detailed features of the flow phenomenon, i.e., like the corner vortices.

The application of the ISPH method to the natural convection problem in a square enclosure from a heated cylinder shows the promising capability of the method to model a complex geometry without mesh generation. The results obtained are in good agreement with results from the previous studies which are based on alternative numerical method.

The study of mixed convection from a heated and rotating cylinder at using the ISPH method shows that in a confined space the addition of kinetic energy to the system in the form of rotation does not enhance the heat transfer process.

Using a simple method for inlet and outlet treatment, current incompressible SPH method is capable of simulating forced convection in external flow without having to prescribe any boundary condition for the lateral boundaries.

Acknowledgements

The authors would like to express their gratitude for the financial support from National Science Council, Taiwan (No: NSC 101-2212-E-011-043) and also graduate scholarship from National Taiwan University of Science and Technology.

References

Angeli, D., Levoni, P. and Barozzi, G.S. (2008), "Numerical predictions for stable buoyant regimes within a square cavity containing a heated horizontal cylinder", *Int. J. Heat Mass Transfer*, **51** (3-4), 553-565.

Bonet, J. and Lok, T.S. (1999), "Variational and momentum preservation aspects of Smooth Particle Hydrodynamic formulations", *Comput. Meth. Appl. Mech. Eng.*, **180**(1-2), 97-115.

Brookshaw, L. (1985), "A method of calculating radiative heat diffusion in particle simulations", *Proceedings of the Astronomical Society of Australia*, **6**(2), 207-210.

Chandrasekhar, S. (1961), *Hydrodynamic and Hydromagnetic Stability*, Clarendon Press , Oxford, UK.

Chern, M., Borthwick, A. and Taylor, R.E. (2006), "Pseudospectral element model for free surface viscous flows", *Int. J. Numer. Meth. Heat Fluid Flow*, **15**(6), 517-554.

Chorin, A.J. (1968), "Numerical solution of the Navier-Stokes equations", *Math. Comput.*, **22**(104), 745-762.

Cleary, P.W. (1998), "Modeling confined multi-material heat and mass flows using SPH", *Appl. Math. Model.*, **22**(12), 981-993.

Cleary, P.W. and Monaghan, J.J. (1999), "Conduction modelling using smoothed particle hydrodynamics", *J. Comput. Phys.*, **148**(1), 227-264.

Coutanceau, M. and Bouard, R. (1977), "Experimental determination of the main features of the viscous flow in the wake of a circular cylinder in uniform translation. Part 1. Steady flow", *J. Fluid Mech.*, **79**(2), 231-256.

Cummins, S.J. and Rudman, M. (1999), "An SPH projection method", *J. Comput. Phys.*, **152**(2), 584-607.

Ghaddar, N.K. and Thiele, F. (1994), "Natural convection over a rotating cylindrical heat source in a rectangular enclosure", *Numer. Heat Tr. A-Appl.*, **26**(6), 701-717.

Gingold, R.A. and Monaghan, J.J. (1977), "Smoothed particle hydrodynamics-theory and application to non-spherical stars", *Mon. Not. R. Astron. Soc.*, **181**, 375-389.

Goda, K. (1979), “A multistep technique with implicit difference schemes for calculating two-or three-dimensional cavity flows”, *J. Comput. Phys.*, **30**(1), 76-95.

Gray, D.D. and Giorgini, A. (1976), “The validity of the Boussinesq approximation for liquids and gases”, *Int. J. Heat Mass Transfer*, **19**(5), 545-551.

Hu, X.Y. and Adams, N.A. (2007), “An incompressible multi-phase SPH method”, *J. Comput. Phys.*, **227**(1), 264-278.

Kim, J. and Choi, H. (2004), “An immersed-boundary finite-volume method for simulation of heat transfer in complex geometries”, *J. Mech. Sci. Tech.*, **18**(6), 1026-1035.

Kum, O., Hoover, W.G. and Posch, H.A. (1995), “Viscous conducting flows with smooth-particle applied mechanics”, *Phys. Review E*, **52**(5), 4899-4908.

Lastiwka, M., Quinlan, N.J. and Basa, M. (2009), “Permeable and non-reflecting boundary conditions in SPH”, *Int. J. Numer. Meth. Fluid.*, **61**(7), 709-724.

Lee, E.S., Moulinec, C., Xu, R. and Violeau, D. (2008), “Comparisons of weakly compressible and truly incompressible algorithms for the SPH mesh free particle method”, *J. Comput. Phys.*, **227**(18), 8417-8436.

Liu, G.R. and Liu, M.B. (2003), *Smoothed Particle Hydrodynamics a Meshfree Particle Method*, World Scientific, Singapore.

Liu, M.B. and Liu, G.R. (2010), “Smoothed particle hydrodynamics (SPH): an overview and recent developments”, *Arch. Comput. Meth. Eng.*, **17**(1), 25-76.

Lucy, L.B. (1977), “A numerical approach to the testing of the fission hypothesis”, *Astronom. J.*, **82**(12), 1013-1024.

Monaghan, J.J. (1992), “Smoothed particle hydrodynamics”, *Ann. Review Astronom. Astrophys.*, **30**, 543-574.

Monaghan, J.J. (2012), “Smoothed particle hydrodynamics and its diverse applications”, *Ann. Review Fluid Mech.*, **44**, 323-346.

Monaghan, J.J. (1989), “On the problem of penetration in particle methods”, *J. Comput. Phys.*, **82**(1), 1-15.

Morris, J.P., Fox, P.J. and Zhu, Y. (1997), “Modeling low Reynolds number incompressible flowsusing SPH”, *J. Comput. Phys.*, **136**(1), 214-226.

Moukalled, F. and Acharya, S. (1996), “Natural convection in the annulus between concentric horizontalcircular and square cylinders”, *J. Thermophys. Heat Transfer*, **10**(3), 524-531.

Noor, D.Z., Chern, M.J. and Horng, T.L. (2009), “An immersed boundary method to solve fluid-solidinteraction problems”, *Comput. Mech.*, **44**(4), 447-453.

Oger, G. *et al*. (2007), “An improved SPH method: Towards higher order convergence”, *J. Comput. Phys.*, **225**(2), 1472-1492.

Ouertatani, N., Ben Cheikh, N., Ben Beya, B. and Lili, T. (2008), “Numerical simulation of two-dimensional Rayleigh–Bénard convection in an enclosure”, *Comptes Rendus Mécanique*, **336**(5), 464-470.

Pacheco-Vega, A., Pacheco, J.R. and Rodic, T. (2007), “A general scheme for the boundary conditionsin convective and diffusive heat transfer with immersed boundary methods”, *J. Heat Transfer*, **129**(11), 1506-1516.

Pan, D. (2006), “An immersed boundary method on unstructured cartesian meshes for incompressible flows with heat transfer”, *Numer. Heat Transfer*, **49**(3), 277-297.

Peng, Y., Chew, Y.T. and Shu, C. (2003), “Numerical simulation of natural convection in a concentricannulus between a square outer cylinder and a circular inner cylinder using the Taylor-series-expansion and least-squares-based lattice Boltzmann method”, *Phys. Review E*, **67**(2), 026701.

Rosenfeld, M., Kwak, D. and Vinokur, M. (1991), “A fractional step solution method for the unsteady incompressible Navier-Stokes equations in generalized coordinate systems”, *J. Comput. Phys.*, **94**(1), 102-137.

Shao, S. and Lo, E.Y. (2003), “Incompressible SPH method for simulating Newtonian and non-Newtonian flows with a free surface”, *Adv. Water Resour.*, 26(7), 787-800.

Shu, C. and Zhu, Y. (2002), “Efficient computation of natural convection in a concentric annulus between an outer square cylinder and an inner circular cylinder”, *Int. J. Numer. Meth. Fluids*, **38**(5), 429-445.

Sigalotti, L., Klapp, J., Sira, E., Meleán, Y. and Hasmy, A. (2003), "SPH simulations of time-dependent Poiseuille flow at low Reynolds numbers", *J. Comput. Phys.*, **191**(2), 622-638.

Szewc, K., Pozorski, J. and Tanière, A. (2011), "Modeling of natural convection with smoothedparticle hydrodynamics: Non-Boussinesq formulation", *Int. J. Heat Mass Transfer*, **54**(23-24), 4807-4816.

Temam, R. (1968), "Une m´ethode d'approximation de la solution des ´equations de Navier-Stokes", *Bull. Soc. Math. Fr.*, **96**, 115-152.

Xu, R., Stansby, P. and Laurence, D. (2009), "Accuracy and stability in incompressible SPH (ISPH)based on the projection method and a new approach", *J. Comput. Phys.*, **228**(18), 6703-6725.